Thermal conductivity of ZrO_2-4 mol%Y_2O_3 thin coatings by pulsed thermal imaging method

Byung-Koog Jang, Jiangang Sun, Seongwon Kim, Yoon-Suk Oh, Sung-Min Lee, Hyung-Tae Kim

PII: S0257-8972(15)00570-8
DOI: doi: 10.1016/j.surfcoat.2015.09.065
Reference: SCT 20656

To appear in: *Surface & Coatings Technology*

Received date: 25 March 2015
Revised date: 11 September 2015
Accepted date: 12 September 2015

Please cite this article as: Byung-Koog Jang, Jiangang Sun, Seongwon Kim, Yoon-Suk Oh, Sung-Min Lee, Hyung-Tae Kim, Thermal conductivity of ZrO_2-4 mol%Y_2O_3 thin coatings by pulsed thermal imaging method, *Surface & Coatings Technology* (2015), doi: 10.1016/j.surfcoat.2015.09.065

MANUSCRIPT REPORT FORM

PAPER NUMBER (if known)； #AP20

TITLE OF PAPER: Thermal Conductivity of ZrO_2-4mol%Y_2O_3 Thin Coatings by Pulsed Thermal Imaging Method

PRESENTING AUTHOR: Byung-Koog Jang

FULL MAILING ADDRESS: High Temperature Materials Unit,
National Institute for Materials Science (NIMS)
1-2-1 Sengen, Tsukuba, Ibaraki 305-0047, Japan

TELEPHONE: +81-29-859-2453(direct)

FAX: +81-29-859-2401

E-MAIL: JANG.Byungkoog@nims.go.jp

CORRESPONDING AUTHOR: Byung-Koog Jang

FULL MAILING ADDRESS: High Temperature Materials Unit,
National Institute for Materials Science (NIMS)
1-2-1 Sengen, Tsukuba, Ibaraki 305-0047, Japan

TELEPHONE: +81-29-859-2453(direct)

FAX: +81-29-859-2401

E-MAIL: JANG.Byungkoog@nims.go.jp

Thermal Conductivity of ZrO_2-4mol%Y_2O_3 Thin Coatings by Pulsed Thermal Imaging Method

Byung-Koog Jang[a),*] Jiangang Sun[b)],

Seongwon Kim[c)], Yoon-Suk Oh[c)], Sung-Min Lee[c)] and Hyung-Tae Kim[c)]

[a)] High-Temperature Materials Unit, National Institute for Materials Science

1-2-1 Sengen, Tsukuba, Ibaraki 305-0047, Japan

[b)] Argonne National Laboratory,

9700 South Cass Avenue Argonne, IL 60439, USA

[c)] Engineering Ceramic Center,

Korea Institute of Ceramic Engineering and Technology,

30 Gyeongchung Rd, Sindun-myeon, Icheon 467-843, Korea

* Corresponding author:

Tel.: +81-29-859-2453; Fax: + 81-29-859-2401

E-mail address: JANG.Byungkoog@nims.go.jp (B.K. Jang)

Abstract

Thin ZrO_2-4mol% Y_2O_3 coatings were deposited onto ZrO_2 substrates by electron beam-physical vapor deposition. The coated samples revealed a feather-like columnar microstructure. The main phase of the ZrO_2-4mol% Y_2O_3 coatings was the tetragonal phase. To evaluate the influence of the coating's thickness on the thermal conductivity of thin ZrO_2-4mol% Y_2O_3 coatings, the pulsed thermal imaging method was employed to obtain the thermal conductivity of the coating layer in the two-layer (coating and substrate) samples with thickness between 56 and 337 micrometers. The thermal conductivity of the coating layer was successfully evaluated and compared well with those obtained by the laser flash method for similar coatings. The thermal conductivity of coatings shows an increasing tendency with an increase in the coating's thickness.

Key words: electron beam-physical vapor deposition; ZrO_2; Y_2O_3; pulsed thermal imaging method; thermal conductivity

1. Introduction

Thermal barrier coatings (TBCs) have received much attention because they increase the thermal efficiency of gas turbine engines by increasing the gas turbine inlet temperature and reducing the amount of cooling air required for hot section components. Among the various coating processes for producing TBCs, Electron Beam-Physical Vapor Deposition (EB-PVD) is widely used because, as compared with plasma sprayed coatings, it has several advantages, including a high deposition rate, use of high melting point oxides, and excellent thermal shock resistance behavior due to the porous columnar microstructure of the coatings [1–3].

Of the various physical properties of TBC materials, thermal conductivity is the most important thermal property. The conductivity of TBCs can be measured by several methods. The most commonly used is the laser flash method, in which a laser flash is applied on one surface of a plate specimen, and the thermal transient on the opposite surface is measured by an infrared detector to determine the coating's thermal diffusivity (α) based on the theory of Parker et al. [4].

Thermal conductivity (k) is then calculated from the known heat capacity (ρc) by $k = \alpha \rho c$, where ρ is the density, and c is the specific heat. Because a laser flash requires two-sided access, TBC specimens are usually prepared as stand-alone (single layer)

coatings [5]; alternatively, two-layer TBC specimens with thin substrates may also be used [6,7]. The laser flash is a standard test method with high absolute accuracy. However, caution is needed when testing thin TBCs due to inadequate testing conditions such as nonlinearity [8] and the flash duration effect [9]. Although such testing errors can be avoided, a major concern comes from the use of the laser flash for studying sintering or the effect of thermal exposure on TBCs due to the required specimen configuration/preparation that makes them unrepresentative of real application conditions (i.e., TBC coatings on real substrates). Because sintered stand-alone TBCs and TBCs on real substrates normally have significantly different thermal properties [10], laser flash measurements on stand-alone or specially prepared two-layer TBC specimens may not provide accurate TBC sintering effects in conditions of real engine operation.

Recognizing potential difficulties in the laser flash method, one-sided methods are more appropriate for TBC property measurement because they can be used to test real TBC specimens or TBC-coated engine components. Three one-sided methods have been developed specifically for measuring TBC thermal properties: the phase of photo-thermal emission analysis method (PopTea) [11], the laser flash thermography method (LFT) [12], and the pulsed thermal imaging-multilayer analysis method (PTI-MLA) [13]. In PopTea, a modulated laser heating is provided on the coating

surface, and the phase change of the thermal emission over a range of modulation frequencies is measured by an infrared detector to determine both the coating's conductivity (k) and heat capacity (ρc). In LFT, a flash laser source with a typical Gaussian profile is applied on the coating surface, and the surface temperature evolution is measured by an infrared camera to determine thermal diffusivities in both in-depth and in-plane directions. In PTI-MLA, a thermal pulse is applied uniformly on the TBC's surface, and the surface temperature transient is imaged by an infrared camera and used to calculate the distributions of both the thermal conductivity and the heat capacity over the entire TBC surface. When applying these one-sided methods, at least two differences should be considered. First, both PopTea and LFT can only be used for TBCs on a thick substrate (theoretically, for a semi-infinite substrate) but not a thin substrate (such as a thicker specimen with 337 μm coatings thickness in this study); while PTI-MLA can be applied to all TBC specimens. Second, PopTea and LFT can only provide a single set of average TBC properties from each experiment, while PTI-MLA provides the distributions (or images) of the measured properties over the entire coating surface from a single experiment. The PTI-MLA method has been validated to be capable of achieving an absolute measurement accuracy of <2% [13].

The purpose of the present work is to evaluate the thermal conductivity derived from double-layer samples (coatings and a substrate) using PTI-MLA as a function of the

thickness of ZrO_2-4mol%Y_2O_3 coatings deposited by EB-PVD. This is the first investigation of using the PTI-MLA method for TBC thermal conductivity measurements for a wide range of TBC coating and ZrO_2 substrate thicknesses.

2. Experimental procedures

EB-PVD coatings were obtained by depositing 4 mol% Y_2O_3-stabilized ZrO_2 onto disc-shaped dense zirconia substrates 10.0 mm in diameter and 0.5 and 1 mm in thickness using same composition (Tosho Co., Japan). To eliminate the influence of interfaces and bond coat layers on the thermal conductivity, a bond coat was not deposited. Deposition by EB-PVD was obtained from a water-cooled copper crucible using a commercially available ZrO_2-4mol%Y_2O_3 ingot. For each coating, a plate-type zirconia substrate was inserted into a special holder assembly and placed under a vacuum. The substrate was first heated to 1000°C in a preheating chamber using graphite heating elements. An electron beam evaporation process was carried out in a coating chamber to deposit the film at a rate of 5 μm/min under a vacuum of 10^{-4} Pa using a 45 kW electron gun and a substrate rotation speed of 5 rpm. The coating thicknesses of four samples were in a range of 56~337 μm. The coating layer was found to be well bonded with the substrate (as seen in Fig. 2a); therefore any thermal

resistance at the interface, if exists, is expected to be negligible. The microstructure of the coated specimen was observed by scanning electron microscopy (SEM). Raman spectroscopy was used to determine the crystal structures of coated specimens. The surface roughness of coated layers was analyzed using both a surface roughness tester and a laser microscope (Keyence, VK-8510).

The conductivity (k) and the heat capacity (ρc) of four ZrO_2-4mol%Y_2O_3 EB-PVD TBC specimens were measured by the PTI-MLA method at room temperature. The experimental data were obtained using a system illustrated in Fig. 1(a). During an experiment, a pulsed thermal energy from the optical illumination in the 0.3-2.5 μm wavelength band of a photographic flash lamp [13] was applied on the specimen surface, and a series of thermal images, i.e., surface temperature images, was recorded by an infrared camera. Because TBCs are optically translucent to visible and infrared light, a thin graphite coat was painted on the TBC surface to prevent optical penetration into the TBC's volume. The graphite coat was observed to be well bonded to the TBC coating and its thickness was estimated to be within 1~2 μm; such coat has been verified to have negligible effect to measurement accuracy [14]. Detailed description of this and two other graphite coats, their application and removal, and their effect to the thermal property measurement for various types of TBCs can be found in [25]. The experimental data provide surface temperature transients as a

function of time for all surface positions of a TBC specimen. At each surface position, the surface temperature experiences an initial rapid increase due to the deposition of pulsed thermal energy onto the surface, then gradually decays as surface heat is transferred inside the material by heat conduction, and eventually approaches a constant as heat is uniformly distributed within the specimen's volume. These characteristics are best observed by plotting the slope of the surface temperature, T, with the time, t, in a log scale, $d(\ln T)/d(\ln t)$, which is a dimensionless parameter. Figure 1(b) shows the slope curves for a one-layer and a two-layer material calculated based on a theoretical multilayer model under ideal pulsed thermal imaging conditions (i.e., zero flash duration) and perfect bonding between the layers (i.e., no thermal resistance at interface). The slope has a characteristic −0.5 value in the early times for both one- and two-layer materials, indicating that heat is transferred within a homogeneous material. The two-layer material, however, has a negative slope peak, "interface peak," within a later period of decay. The interface peak was induced by the increased heat transfer rate when the internal heat is conducted from a low-conductivity material (coatings) to a high-conductivity material (substrate). This peak is the most important feature utilized by PTI-MLA to determine the coating properties. In particular, when the substrate's thermal effusivity (e) = $(k\rho c)^{1/2}$ (and also its thickness if the substrate is thin) is known, the peak magnitude uniquely determines

the coating's thermal effusivity, and the peak time is directly related to the coating's diffusivity and thickness [13]. Therefore, with a known coating thickness, both the coating conductivity, k, and the heat capacity, ρc, can be determined simultaneously. This data regression process was automated for all pixels, and the final results were presented as images of the predicted coating properties. Average thermal properties for each specimen were then obtained from the images. The measurement accuracy of the PTI-MLA method has been evaluated for EB-PVD and plasma sprayed TBCs on substrate of various materials and thicknesses [13]. Many experimental conditions and sample material parameters may affect measurement accuracy. However, the PTI-MLA method has accounted for all those effects and achieved a typical measurement error of <3% for all samples.

To compare the thermal conductivity of the free-standing coating samples, the laser flash method was also used to evaluate the accuracy of the PTI-MLA method.

3. Results and discussion

3.1. Fabrication of ZrO_2-4mol%Y_2O_3 coatings by EB-PVD

Figure 2 is a typical SEM micrograph of a ZrO_2-4 mol% Y_2O_3 coating fabricated

by EB-PVD. The surfaces of coatings deposited onto the substrates have a crystalline columnar texture with all columnar grains oriented in the same direction, i.e., perpendicular to the substrate, and with predominantly open micro- and nanoporosity [15]. The gaps between the columns could be clearly observed in Fig. 2(b). The columns are all aligned in the same direction, perpendicularly to the substrate. These gaps contribute to the total porosity of the coatings. On both sides of the columnar grains, a pronounced dendritic structure that contains many micropores as well as nanopores was formed [15,16]. The columnar microstructure characteristic of EB-PVD imparts thermal conductivity.

Typical microstructures and a laser microscope image of the top surface of ZrO_2-4 mol% Y_2O_3 coatings are shown in Fig. 3. The top surfaces of EB-PVD coatings consist of square-pyramidal or cone-like grains, as shown in Fig. 3(a). Coated specimens with a crystalline columnar texture in all columnar grains have a predominantly open microporosity. The deposited surface has a rough appearance because the crystal faces form square-pyramid-like tips protruding from the ends of the columnar grains as shown in Fig. 3(b). The roughness is approximately 3.27 μm.

Figure 4 shows the Raman spectra of the top surfaces of ZrO_2-4 mol% Y_2O_3 coatings. This indicates that the observed phase in the coatings is the tetragonal phase of zirconia, as the spectra are dominated by relatively sharp tetragonal Raman modes

(indicated by arrows in Fig. 4) [17].

3.2. Thermal properties by the PTI-MLA method

In this study, all experiments were conducted at an imaging speed of 1068 Hz for 2 seconds. Figure 5(a) shows average surface temperature slope data for coatings specimens (a)~(d). All slope curves exhibit another negative peak at an early time $t \approx 8$ ms. This peak was due to the flash duration [13], which was measured to be 1.8 ms for the flash lamp used in this study. The flash duration has been accounted for in the PTI-MLA method, so it has no or negligible effect on TBC thermal property measurement [14]. In Fig. 5(a), the interface peak time increases from <10 ms to >100 ms in ascending order for specimens (a)~(d), respectively, due to the increase of the TBC thickness (peak time is approximately proportional to the TBC thickness square [13]). Specimen (c)'s slope took a much longer time to return to near zero because its substrate was twice as thick as that of other specimens (1 mm vs. ~0.5 mm), so it required a longer time for its temperature to become uniform (i.e., steady state). The surface temperatures of all specimens displayed a slight decrease at ~1 s (i.e., small negative slope). This was because their back surfaces were taped on a supporting low-conductivity plate during the test, so there existed a small heat leak into the plate;

however, this small heat leak did not affect the TBC property measurements because it happened much later. In general, the PTI-MLA method uses only the experimental data around the interface peak to predict TBCs' thermal properties [13,14]. Figure 5(b) shows measured and fitted curves for a typical pixel in coating specimens (a)-(d). It is evident that the fitting around all interface peaks was very good; the miner deviations within an early time of generally <10ms were probably due to the presence of surface roughness and air gaps between the coating columns.

Figure 6 shows the measured thermal conductivity (k) and the heat capacity (ρc) images of the four TBC specimens (a)~(d). The thermal property images are generally uniform, indicating uniform coating thickness and material. Some images show minor property variations at the left vertical edge; this was due to edge heating by the flash lamp, as it was placed on the left side during the experiments. Most thermal property images display small, localized variations of either higher or lower values; this was due to the presence of surface defects (small pits or droplets) on the coating surfaces. The average coating properties were extracted from these images in areas away from the edges and surface defects; they are listed in Table 1 and plotted in Fig. 7 as a function of the TBC's thickness. The measured TBC thermal conductivities for ZrO_2-4mol%Y_2O_3 specimens (a)~(d) in Table 1 and Fig. 7 show a clear increase with TBC thickness, which is consistent with the data reported in the literature [18].

The simultaneous measurement of both thermal conductivity and heat capacity for the same specimens by PTI-MLA allows for an examination of combined TBC conductivity and density (and porosity) variations with the TBC depth. The TBC density (ρ) can be calculated directly from its heat capacity because the TBC's specific heat (c) is affected only by the material's composition and, thus, is a constant for these specimens. Based on a commonly used TBC-specific heat value, c = 480 J/kg·K [19, 20], predicted TBC densities for the specimens (a)~(d) are listed in Table 1. Further, because the bulk density of 100% dense ZrO_2-4mol%Y_2O_3 material is also a constant, ρ_s = 6.05 g/cm^3, the porosities (1-ρ/ρ_s) of these specimens can also be calculated as listed in Table 1.

The results in Table 1 show that TBC density increases when TBC thickness is >100 μm (or, correspondingly, with a decrease in TBC porosity). However, TBC density is highest when TBC thickness is very thin, at 56 μm for specimen (a). This result seems to be counterintuitive, but it could be explained by considering the coating microstructural variations along its depth. EB-PVD TBC microstructure exhibits a columnar structure with porosity between the columns (see Fig. 2; also Fig. 2 in [18]).However, there is a drastic difference in the microstructure between an inner and an outer zone: the inner coating within ~50 μm thickness from the interface has a fine-grained structure with numerous grain boundaries, while the outer coating consists

of large columnar grains with intercolumnar porosities mostly aligned perpendicularly to the surface [18]. Although accurate measurement of coating density within the inner zone appears to be unavailable, the inner zone is generally considered to be denser and impermeable to gas infiltration [10], having much lower thermal conductivity than that in the outer zone (by a factor of 2~5 [18,21]). Based on these observations, it is reasonable to understand that specimen (a) has a higher density but a lower thermal conductivity because, at a coating thickness of 56 μm, it consists of only an inner-zone microstructure.

The simultaneous measurement of both TBC thermal conductivity and heat capacity (or density) also allows for a direct examination of the correlation between them. Figure 8 shows TBC thermal conductivity as a function of heat capacity (or density). This correlation however can only be obtained for TBCs in the outer-zone thickness, i.e., for specimens (b)~(d). Such a restriction was also observed when correlating grain sizes with depth: a linear correlation can be obtained only in the outer-zone depths, as shown in Fig. 4 of [18]. The linear correlation in Fig. 8 demonstrates clearly that the thermal conductivity increase in these specimens was due to the increase of the coating density.

3.3. Comparison of thermal conductivity

Figure 9 shows a comparison of TBC thermal conductivity measured in this study for various coating thicknesses by the present method and the laser flash method [22]. Despite some differences in thermal conductivity values, the general trends for both sets of data are essentially the same. The thermal conductivity of a coating tends to increase with increasing thickness of the coating. As shown in Fig. 9, the thermal conductivity by the present method is in good agreement with the results by the laser flash method [22]. Consequently, this result shows that the present method is a useful method for determining the thermal conductivity of coating layers from the combined coating and substrate specimens when it cannot be measured directly from separated coating layers with thinner thicknesses. In addition, thinner coating layers, below 200 μm thickness, reveal lower thermal conductivity than that of specimens with thicker coatings above 200 μm. It seems likely that the low thermal conductivity of thinner coating layers depends on the microstructural nature of columnar grains.

Figure 10 shows the number of column boundaries per the same area for each ZrO_2-4 mol% Y_2O_3 coating deposited by EB-PVD. The number of column boundaries decreased as the coating thickness increased.

In Fig. 2, the columns are smaller and finer near the substrate area; whereas, they are larger and coarser at the surface area. For this reason, the width and size of

columns for thinner coating layers are small and fine, resulting in many columns. On the contrary, the width and size of columns for thicker coating layers are relatively large and coarse.

Consequently, the thinner coating layers have many column boundaries as compared with those for thicker coating layers. This result affects the mechanism of the thermal conductivity of coatings as follows.

Lower thermal conductivity is generally close to the phonon scattering in the lattice. In other words, phonons interact with imperfections such as dislocation, vacancy, pore boundaries, and grain boundaries, resulting in increased phonon scattering. The phonon mean free path (l_p) is defined by [23, 24]:

$$\frac{1}{l_p} = \frac{1}{l_i} + \frac{1}{l_{gb}} + \frac{1}{l_{vac}} + \frac{1}{l_{strain}} \quad (1)$$

where l_i, l_{gb}, l_{vac}, and l_{strain} are contributions to the phonon mean free path due to interstitials, grain boundaries, vacancies, and lattice strain, respectively. Therefore, grain boundaries affect the phonon mean free path. It seems that the column boundaries in the present coatings are similar to the grain boundaries in sintered materials for the microstructural properties. Therefore, many column boundaries in the present coatings can also contribute to a decrease of the phonon mean free path,

resulting in decreased thermal conductivity of coatings. A study of the effects of column sizes and coating thicknesses of EB-PVD ZrO_2 coatings on thermal conductivity by the laser flash method has also been reported, showing that the thermal conductivity of coatings decreases with increasing grain boundaries as well as higher porosity of columns [18]. Consequently, in the present work, many column boundaries in thinner coating layers below 100 μm significantly reduce the mean free path by phonon scattering, resulting in the reduction of thermal conductivity.

4. Conclusions

Thin ZrO_2-4mol%Y_2O_3 coatings with different coating thicknesses were deposited on a ZrO_2 substrate by EB-PVD. The coating layer had a columnar microstructure with intercolumnar gaps between columnar grains. Nanosized pores could be observed around feather-like grains as well as inside columnar grains.

Thermal conductivity was successfully evaluated by the pulsed thermal imaging method using the combined coatings and a substrate. The thermal conductivity of ZrO_2-4mol%Y_2O_3 shows an increasing tendency with increasing coating thickness. These differences in thermal conductivity between thinner and thicker samples can be explained with variations in the columnar microstructure across the thickness of the

coating characterized by a fine-grained zone near the substrate and a coarse-grained zone at the coating's surface. According to the present results of thermal conductivity, it can be concluded that the pulsed thermal imaging method is useful for determining the thermal conductivity of the coating layer using a combined coating and substrate specimen if the thermal conductivity of a free-standing coated layer with thinner thickness cannot be measured directly.

Acknowledgements

This work was carried out with financial support from NIMS and the fundamental R&D program for strategic core technology of materials funded by the Ministry of Trade, Industry and Energy, Korea. The Argonne National Laboratory work was sponsored by the U.S. Department of Energy, Office of Fossil Energy, the Crosscutting Research Program.

References

[1] U.Schulz, W. Braue, Surf. Coat. Techno. 235 (2013)165.

[2] U. Schulz, O. Bernardi, A. E. Stahl, R. Vassen, D. Sebold, Surf. Coat. Technol. 203

(2008) 160.

[3] C.G. Levi, Current Opinion in Solid State and Mat. Sci., 8 (2004) 77.

[4] W.J. Parker, R.J. Jenkins, C.P. Butler, and G.L. Abbott, J. Appl. Phys., 32 (1961) 1679.

[5] B.K. Jang, H. Matsubara, Scripta Mater., 54 (2006) 1655.

[6] B.K. Jang, M. Yoshiya, N. Yamaguchi, H. Matsubara, J. Mater. Sci., 39 (2004) 1823.

[7] J.G. Sun, in Review of Quantitative Nondestructive Evaluation, eds. D.O. Thompson and D.E. Chimenti, 29 (2009) 458.

[8] H. Wang, R.B. Dinwiddie, J. Thermal Spray Techno., 9 (2000) 210.

[9] J.G. Sun, S. Erdman, Review of Quantitative Nondestructive Evaluation, eds. D.O. Thompson and D.E. Chimenti, 23 (2003) 482.

[10] H.-J. Ratzer-Scheibe, U. Schultz, Surf. Coat. Technol., 201 (2007) 7880.

[11] T.D. Bennett, F.L. Yu, J. Appli. Phys., 97 (2005) 013520.

[12] P.G. Bison, F. Cernuschi, E. Grinzato, S. Marinetti, D. Robba, Infrared Phys. Technol., 49 (2007) 286.

[13] J.G. Sun, J. Heat Transfer, 136 (2014) 081601.

[14] J.G. Sun, in Ceramic Eng. Sci. Proc., eds. S. Widjaja and D. Singh, 32 (2011) 15.

[15] B.K. Jang, H. Matsubara, J. Eur. Ceram. Soc., 26 (2006) 1585.

[16] T.J. Lu, C.G. Levi, H.N.G. Wadley, A.G. Evans, J. Am. Ceram. Soc., 84 (2001) 2937.

[17] B. Alzyab, C.H. Perry, R.P. Ingel, J. Am. Ceram. Soc., 70 (1987) 760.

[18] H.-J. Ratzer-Scheibe, U. Schultz, T. Krell, Surf. Coat. Technol., 207 (2006) 5636.

[19] J.F. Bisson, D. Fournier, M. Poulain, O. Lavigne, R. Mévrel, J. Am. Ceram. Soc., 83 (2000) 1993.

[20] B.K. Jang, J.G. Sun, S.W. Kim, Y.S. Oh, H.T. Kim, Surf. Coat. Technol., 207 (2012) 177.

[21] I.M. Earley, MSc thesis, UMIST, Manchester, 1992.

[22] B.K. Jang, Y. Sakka, N. Yamaguchi, H. Matsubara, H.T. Kim, J. Alloys Compd., 509 (2011) 1045.

[23] K.J. Lawson, J.R. Nicholl, D.S. Rickerby, Adv. in Surf. Eng., 1 (1997) 83.

[24] J.R. Nicholl, K.J. Lawson, A. Johnstone, D.S. Rickerby, Mater. Sci. Forum, 595 (2001) 369.

[25] F. Cernuschi, P. Bison, J.G. Sun, Surface & Coatings Technology, 258 (2014) 284.

Table

Table 1. List of measured average thermo-physical properties of the present samples.

Specimen	Thickness (μm)	k (W/m·K)	ρc (J/cm^3·K)	ρ (g/cm^3)	1-ρ/ρ_s (%)
(a)	56	1.17±0.022	2.10±0.030	4.38	27.6
(b)	102	1.45±0.013	1.93±0.018	4.03	33.4
(c)	210	1.55±0.009	1.97±0.021	4.10	32.3
(d)	337	1.84±0.004	2.07±0.022	4.31	28.7

Figure captions

Fig. 1. Schematics of pulsed thermal imaging of a 2-layer material system; (a) thermal imaging system setup and (b) temperature-derivative data.

Fig. 2. SEM micrographs of ZrO_2-4mol% Y_2O_3 coatings deposited by EB-PVD; (a) overview and (b) magnified view of top area.

Fig. 3. SEM micrograph (a) and laser microscope image (b) of the top surfaces for ZrO_2-4mol%Y_2O_3 coatings; Surface roughness (R_a) is 3.27μm.

Fig. 4. Raman spectra of ZrO_2-4mol% Y_2O_3 coatings deposited by EB-PVD.

Fig. 5. Surface temperature slopes of ZrO_2-4mol%Y_2O_3 coatings as a function of time; (a) measured average curves and (b) comparison of measured and fitted curves for a typical pixel in each coating.

Fig. 6. Measured thermal conductivity (upper) and heat capacity (lower) images of ZrO_2-4mol%Y_2O_3 coatings as a function of coating thickness.

Fig. 7. Measured thermal conductivity and heat capacity of ZrO_2-4mol%Y_2O_3 coatings as a function of coating thickness.

Fig. 8. Thermal conductivity vs. heat capacity of ZrO_2-4mol%Y_2O_3 coatings deposited by EB-PVD.

Fig. 9. Thermal conductivity as a function of coating thickness for ZrO_2-4 mol% Y_2O_3 coatings deposited by EB-PVD.

Fig.10. Density of column boundaries (per 100-μm width) as a function of coating thickness for ZrO_2-4 mol% Y_2O_3 coatings.

Figures

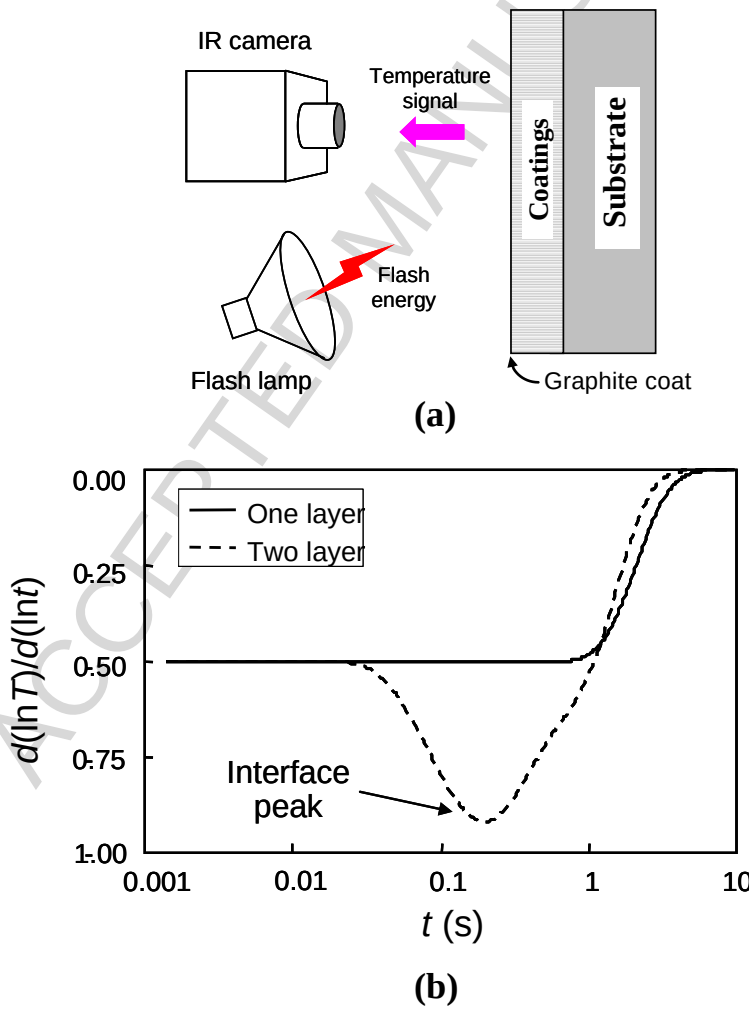

Fig. 1

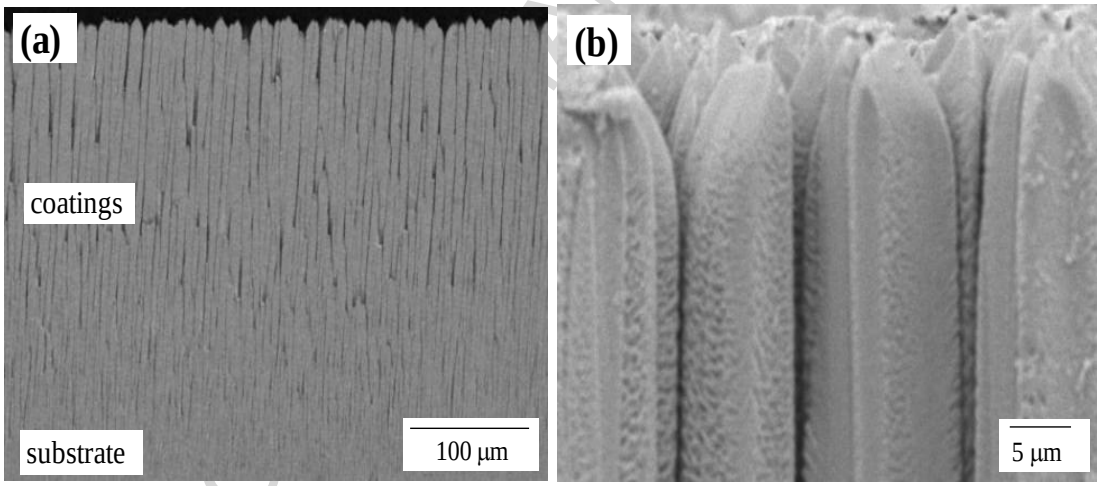

Fig. 2

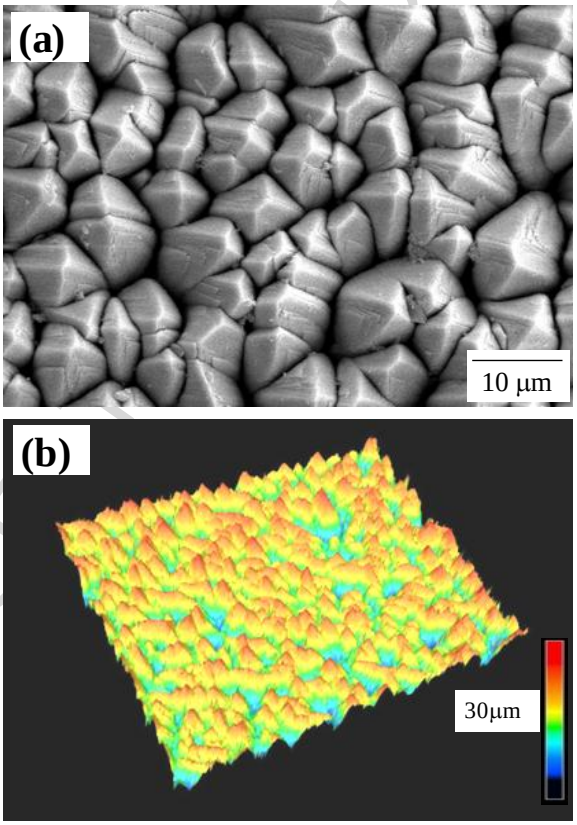

Fig. 3

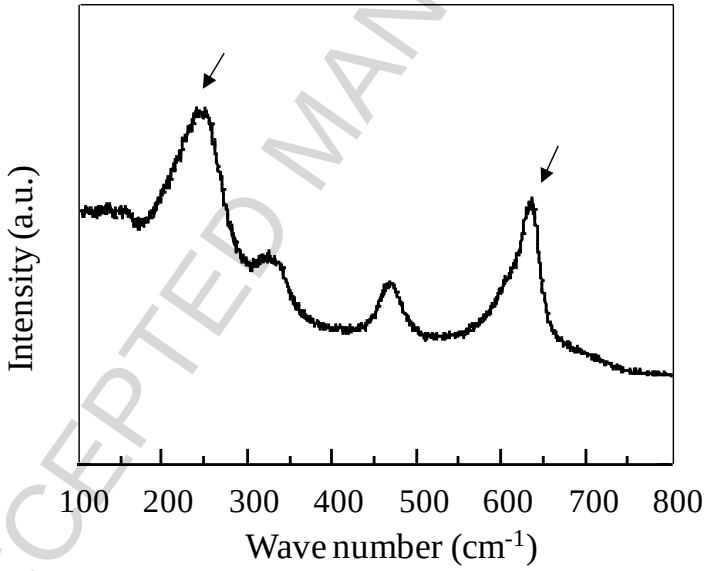

Fig. 4

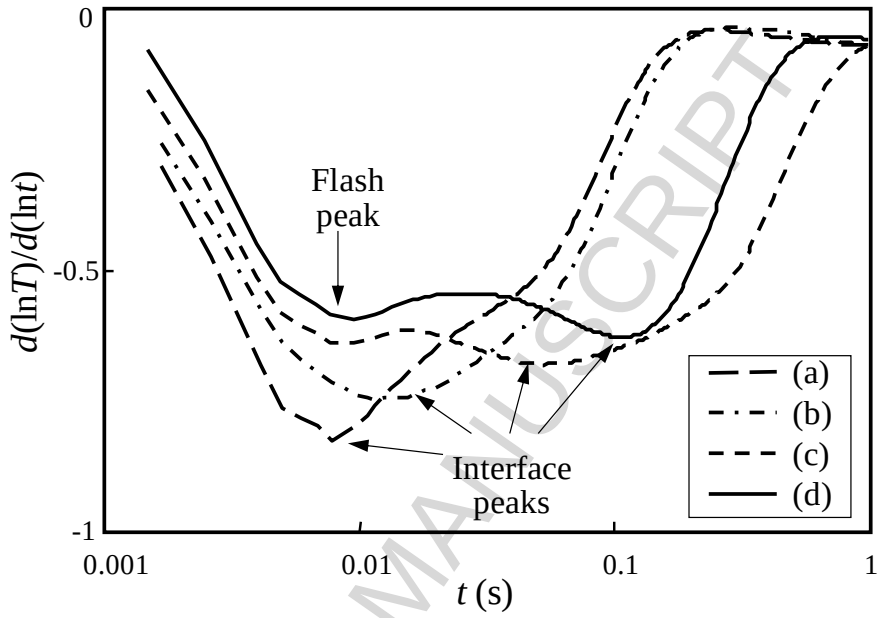

(a)

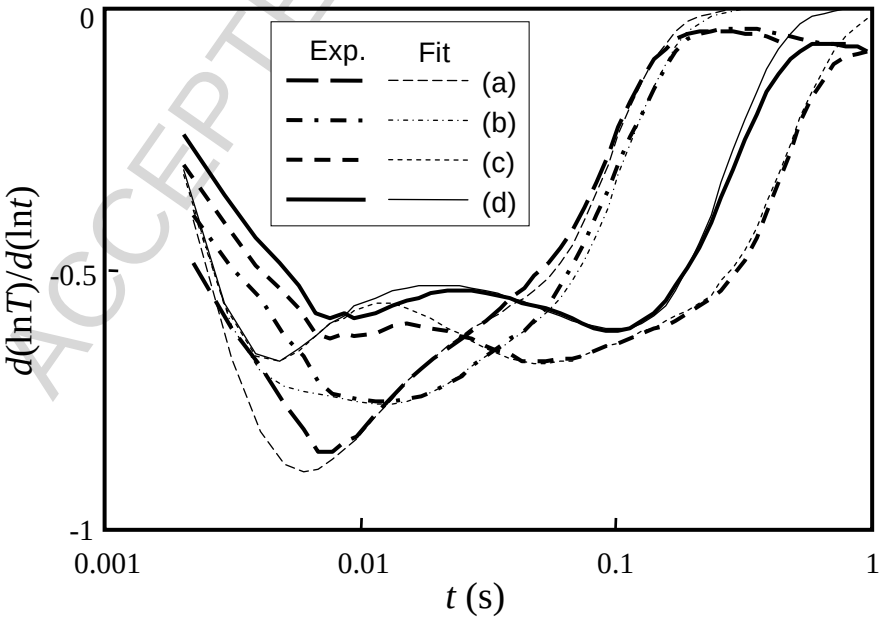

(b)

Fig. 5

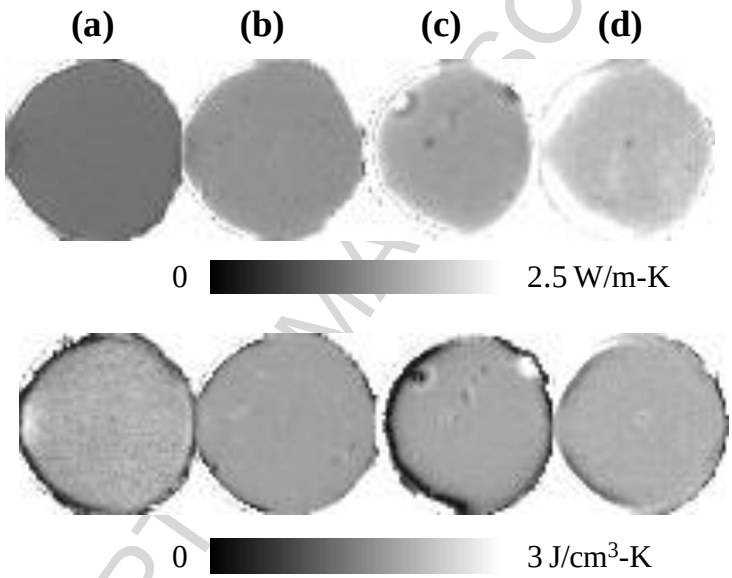

Fig. 6

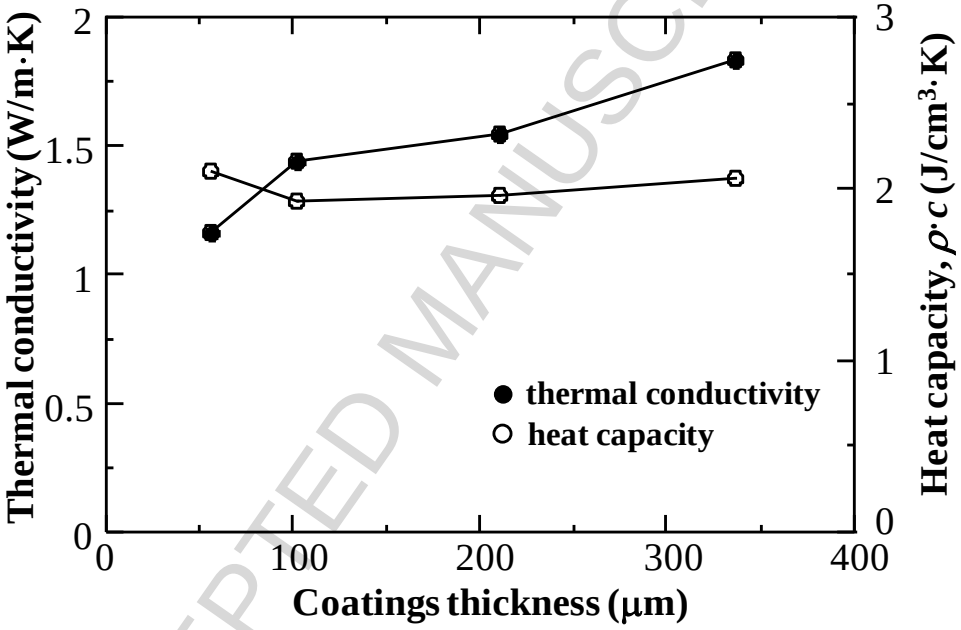

Fig. 7

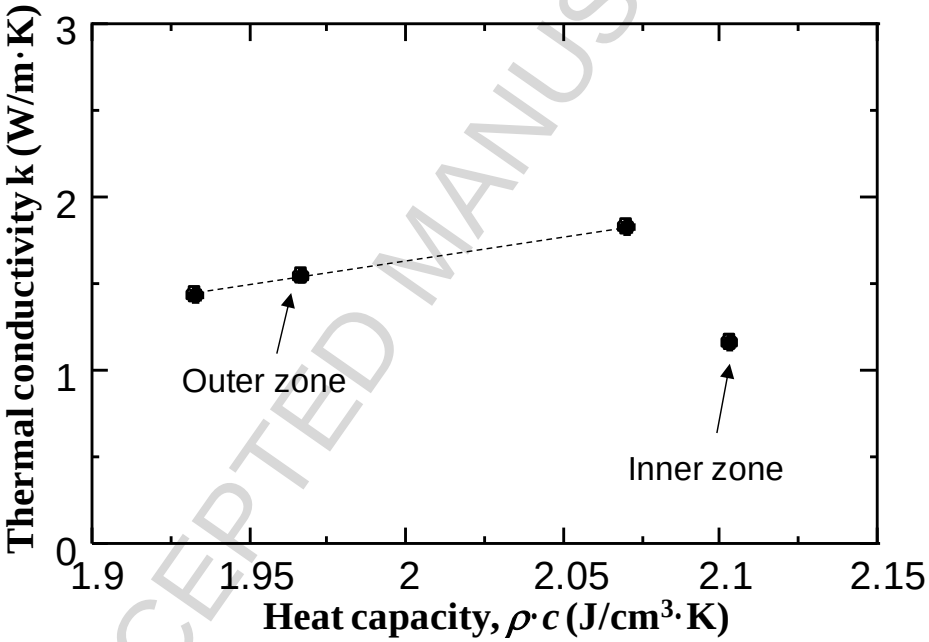

Fig. 8

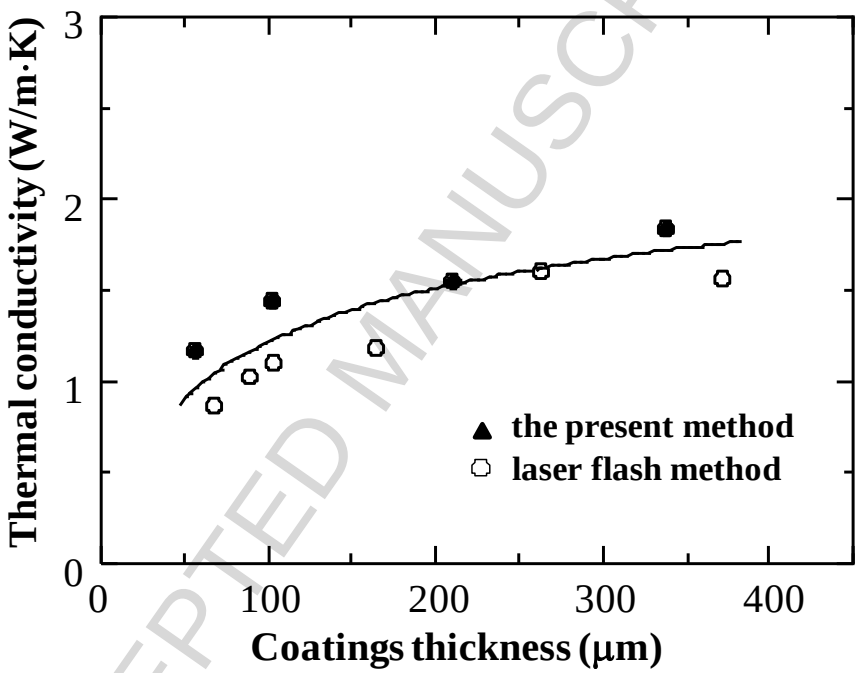

Fig. 9

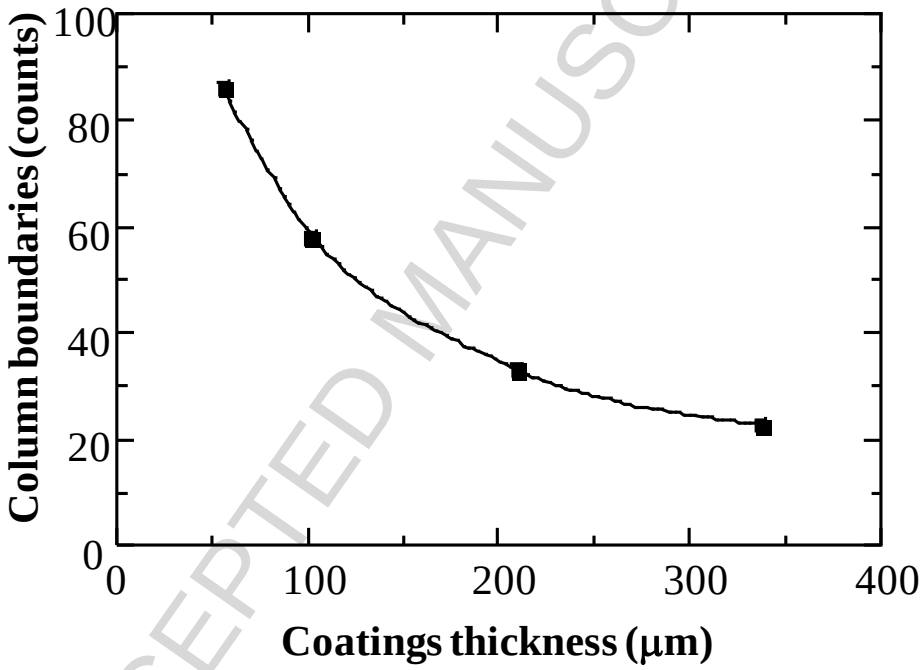

Fig.10

Highlights

- Thin ZrO_2-4mol% Y_2O_3 coatings were deposited by Electron Beam-Physical Vapor Deposition.
- ZrO_2-4mol% Y_2O_3 coatings revealed a feather-like columnar microstructure.
- The thermal conductivity was evaluated from double layers using the thermal image method.
- The thermal conductivity of coatings increased with increasing coating thickness.